Command's internal development effort which led to these design procedures for large-signal broad-band microwave transistor amplifiers. In particular, acknowledgment is given to A. Eykholt, formerly of ABMDA, and to A. Harper of ABMDA, whose confidence in our ideas has been appreciated. Without their enlightened interest and subsequent contractual support, the thorough development of ideas, such as the internal shunt inductor, would not have been fulfilled.

They wish to thank V. Garboushian of Power Hybrids, Inc., for his early initiative in implementing the internal shunt inductor and acknowledging its potential as a broadband matching element in response to our suggestion.

They also wish to thank Dr. E. Belohoubek and A. Presser of RCA, Princeton, N.J., for furnishing the load-pull characterization data which were used in Figs. 1 and 2 and for several helpful comments and suggestions following a review of this paper.

References

[1] E. Belohoubek, A. Rosen, D. Stevenson, and A. Presser, "Hybrid integrated 10-watt CW broad-band power source at *S* band," *IEEE J. Solid-State Circuits (Special Issue on Optoelectronic and Solid-State Microwave Circuits)*, vol. SC-4, pp. 360–366, Dec. 1969.

[2] E. Belohoubek, A. Presser, D. Stevenson, A. Rosen, and D. Zieger, "*S*-band CW power module for phased arrays," *Microwave J.*, vol. 9, pp. 29–34, July 1970.

[3] A. Presser and E. Belohoubek, "1–2 GHz high-power linear transistor amplifier," *RCA Rev.*, vol. 33, pp. 737–751, Dec. 1972.

[4] H. J. Reich, J. G. Skalnik, P. F. Ordung, and H. L. Krauss, *Microwave Principles*. Princeton, N. J.: Van Nostrand, 1957, p. 304.

[5] O. Pitzalis, Jr., and R. A. Gilson, "Broadband gigahertz transistor power amplifiers," in *Digest 1971 IEEE Int. Convention*, pp. 360–361.

[6] "Proposal for the development of a high power broadband transistor amplifier," RCA Tech. Proposal DP 661, prepared by RCA, Princeton, N. J., Mar. 27, 1970, and submitted to the Aeronautical Systems Division (AFSC), Wright-Patterson AFB, Ohio.

[7] G. Matthaei, L. Young, and E. Jones, *Microwave Impedance-Matching Networks and Coupling Structures*. New York: McGraw-Hill, 1964, pp. 360–380.

[8] V. Garboushian, Power Hybrids, Inc., Torrance, Calif., private communication.

[9] "*S*-band solid state power amplifiers," Microwave Semiconductor Corp., Somerset, N. J., U.S. Army Electronics Command, Fort Monmouth, N. J., Contract DAAB07-72-C-0224, Reps. to be published.

[10] "*S*-band solid state power amplifiers," RCA, Princeton, N. J., U.S. Army Electronics Command, Fort Monmouth, N. J., Contract DAAB07-72-C-0225, Reps. to be published.

[11] "Microwave power transistor chip carriers," RCA, Somerville, N. J., U.S. Army Electronics Command, Fort Monmouth, N. J., Contract DAAB07-73-C-0007, Reps. to be published.

[12] "Microwave power transistor chip carriers," Microwave Semiconductor Corp., Somerset, N. J., U.S. Army Electronics Command, Fort Monmouth, N. J., Contract DAAB07-73-C-0008.

[13] H. W. Bode, *Network Analysis and Feedback Amplifier Design*. Princeton, N. J.: Van Nostrand, 1945.

[14] R. Levy, "Explicit formulas for Chebyshev impedance-matching networks, filters, and interstages," *Proc. IEEE*, vol. 53, pp. 939–963, Aug. 1964.

[15] G. Matthaei, "Tables of Chebyshev impedance-transforming networks of low-pass filter form," *Proc. IEEE*, vol. 53, pp. 939–963, Aug. 1964.

[16] E. Schwartz, "Broadband matching of resonant circuits and circulators," *IEEE Trans. Microwave Theory Tech.*, vol. MTT-16, pp. 158–165, Mar. 1968.

[17] T. E. Shea, *Transmission Networks and Wave Filters*. Princeton, N. J.: Van Nostrand, 1929, p. 325.

[18] O. Pitzalis, Jr., and R. A. Gilson, "Tables of impedance-matching networks which approximate prescribed attenuation versus frequency slopes," *IEEE Trans. Microwave Theory Tech.*, vol. MTT-19, pp. 381–386, Apr. 1971.

Characteristics of IMPATT-Diode Reflection Amplifiers

RICHARD W. LATON AND GEORGE I. HADDAD

***Abstract*—The results of an investigation of the gain, stability, phase shift, power addition, saturation, and bandwidth properties of microwave reflection amplifiers which employ IMPATT diodes as the active element, together with the dependence of all these properties upon the device material, doping profile, and operating conditions, are presented. Both Si and GaAs diodes are considered and experimental results demonstrating the validity of the model are provided, together with other experimentally determined characteristics relating gain, saturation, and bandwidth to current density and tuning conditions. Finally, measurements illustrating the degradation of response as a result of subharmonic oscillation are given.**

Manuscript received January 26, 1973; revised April 20, 1973. This work was supported by the Air Force Systems Command's Rome Air Development Center under Contract F30602-71-C-0099.

R. W. Laton was with the Electron Physics Laboratory, Department of Electrical and Computer Engineering, University of Michigan, Ann Arbor, Mich. 48104. He is now with Lincoln Laboratory, Massachusetts Institute of Technology, Lexington, Mass. 02173.

G. I. Haddad is with the Electron Physics Laboratory, Department of Electrical and Computer Engineering, University of Michigan, Ann Arbor, Mich. 48104.

I. Introduction

STABLE reflection gain from an amplifier utilizing an IMPATT diode as the active device was first reported by Napoli and Ikola in 1965 [1]. Subsequently, significant advances have been made in power output [2], operating frequency [3], and gain-bandwidth optimization [4], and several analytical techniques for the design of amplifiers of this type have been described [5]–[8]. These techniques, however, all rely on either experimentally determined device immittance data or on Read [9] model theory, and therefore do not address the problem of optimization of device properties for stable reflection amplifiers.

The purpose of this paper is to provide an improved understanding of the design and analysis of microwave reflection amplifiers employing the negative-resistance property of IMPATT diodes, to demonstrate the validity of that theory by means of experiment and, finally, to utilize the theory to examine the properties of such amplifiers and the dependence

of those properties upon device material, doping profile, temperature, biasing, and circuit conditions.

A model is developed which makes use of discrete device admittance data from realistic large-signal analyses [10], [11] to predict the nonlinear behavior of such amplifiers. A semigraphical analysis of the reflection gain expression provides a visual means of predicting qualitative performance based on device admittance characteristics and leads to the definition of an ideal circuit. Power addition, gain, and bandwidth properties are presented for Si p^+-nn^+, Si n^+-pp^+ and GaAs p^+-nn^+ or Schottky-barrier devices. Broad-banding capability is examined for these structures, as well as for the double-drift region and ideal Read Si diodes. Experimental results are provided verifying the validity of the model and demonstrating the dependence of bandwidth and gain compression on bias current density and tuning conditions.

II. Reflection Gain, Stability, and the Device–Circuit (*D–C*) Diagram

A well-known expression for power gain in a reflection-type amplifier is given by

$$\text{power gain} = |\Gamma|^2 = \left|\frac{Y_{\text{load}} - Y_{\text{device}}^*}{Y_{\text{load}} + Y_{\text{device}}}\right|^2 \tag{1}$$

where Y_{load} is the admittance seen looking away from the active device at some convenient reference plane and Y_{device} is the admittance seen looking toward the device from the same reference plane. The asterisk is used to indicate the complex conjugate.

The admittances in (1) may be represented by vectors from the origin of the admittance plane as shown in Fig. 1. Then the denominator of (1) will be given by the vector labeled $\boldsymbol{D}$[1] in Fig. 1 and the numerator by the vector $\boldsymbol{N}$. That is,

$$\boldsymbol{N} = \boldsymbol{Y}_{\text{load}} - \boldsymbol{Y}_{\text{device}}^* \tag{2}$$

and

$$\boldsymbol{D} = \boldsymbol{Y}_{\text{device}} - (-\boldsymbol{Y}_{\text{load}}). \tag{3}$$

The circles shown in Fig. 1 describe the locus of the tips of the vectors representing $\boldsymbol{Y}_{\text{load}}$, $\boldsymbol{N}$, and $-\boldsymbol{D}$ as the load is varied in such a manner that $|\boldsymbol{D}|$ remains constant for a fixed value of Y_{device} in the second quadrant. Inspection of Fig. 1 reveals that when $|\boldsymbol{D}|$ is small relative to $|\boldsymbol{Y}_{\text{device}}|$, the variation in $|\boldsymbol{N}|$ will be small as the load admittance is varied along the arc representing a constant magnitude of $\boldsymbol{D}$ and that $|\boldsymbol{D}|$ will also be small relative to $|\boldsymbol{N}|$. Thus for device operation anywhere except very close to the origin, large gain, which implies $|\boldsymbol{D}|$ smaller than $|\boldsymbol{N}|$, means that $|\Gamma|^2$, as given by (1), will depend in a very sensitive manner on $1/|\boldsymbol{D}|$, and will be relatively unaffected by $|\boldsymbol{N}|$. Similarly, for a fixed load admittance the same dependence upon $1/|\boldsymbol{D}|$ characterizes the saturation of gain as Y_{device} changes, for example, with a change in bias or RF drive level.

Finally, it should be pointed out that in the limit as $|\boldsymbol{D}|$ approaches zero, the power gain becomes infinite and oscillation will occur. The condition $|\boldsymbol{D}| = 0$ requires that $Y_{\text{load}} = -Y_{\text{device}}$ which is a rather well-known condition for oscillation. This important dependence of gain on $1/|\boldsymbol{D}|$ means that a great deal of insight into gain, bandwidth, and stability behavior can be obtained from a complex plane representation of the diode admittance as a function of RF voltage and frequency together with the negative locus of the circuit admittance versus frequency. Such a plot, which will hereafter be referred to as a device–circuit (*D–C*) diagram, is shown in Fig. 2.

[1] All symbols that appear boldface in text appear with an arrow above them in the figure

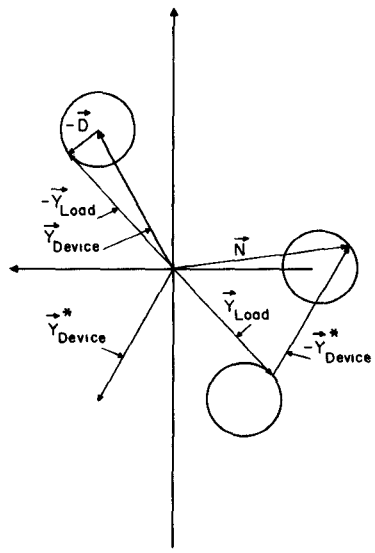

Fig. 1. Complex plane representation of admittances pertinent to reflection gain.

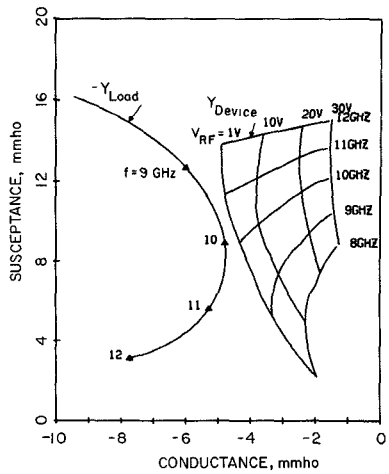

Fig. 2. *D–C* diagram for amplifier example 1. (5-μm Si Read diode; area $= 1 \times 10^{-4}$ cm^2; $J_{dc} = 500$ A/cm^2; one 32-Ω slug $\lambda/4$ at 10 GHz 4 mm from diode flange.)

For this case, referred to hereafter as amplifier example 1, the diode is an Si Read device with an assumed area of 10^{-4} cm^2 4-μm drift length 1-μm avalanche region width and is biased at a current density of 500 A/cm^2. The curve labeled $-Y_{\text{load}}$ is the calculated response presented by a 32-Ω coaxial slug one quarter-wavelength long at 10 GHz, located 4 mm from the diode flange in a 50-Ω coaxial cavity.

The reference plane for the admittances shown in Fig. 2 has been taken on the semiconductor chip itself using an equivalent circuit for the diode package and the coaxial cavity mount, as determined by Greiling and Haddad [10].

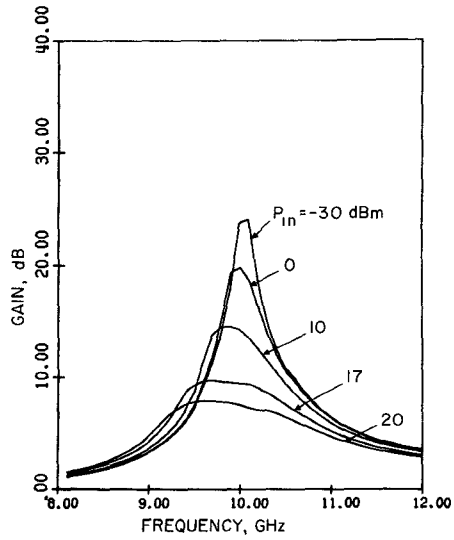

Fig. 3. Gain versus frequency for several values of input power (amplifier example 1).

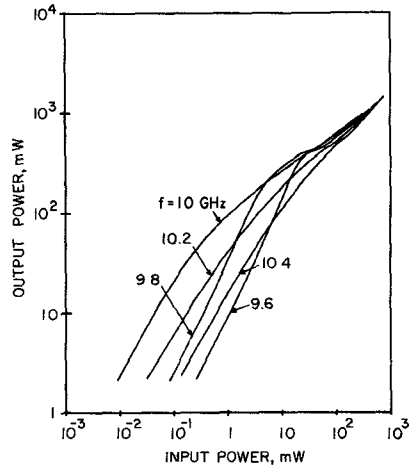

Fig. 4. Output power versus input power for several frequencies (amplifier example 1).

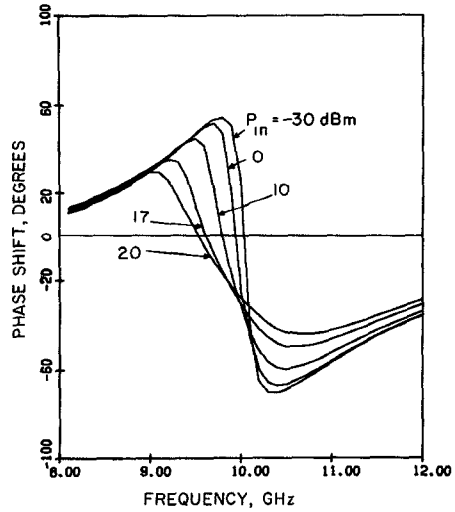

Fig. 5. Phase shift versus frequency at several input power levels (amplifier example 1).

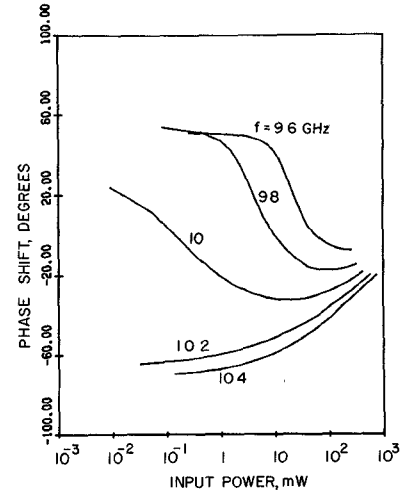

Fig. 6. Phase shift versus input power at several frequencies (amplifier example 1).

With the restriction that device admittance remains in the second quadrant somewhat distant from the origin, the *D–C* diagram may be analyzed to reveal the following expected characteristics of the amplifier it represents.

First, stable operation is assured since there is no common frequency intersection of device and circuit curves at any frequency for which the device admittance has a negative real part. It must be pointed out, however, that since negative resistance can be induced under large-signal conditions at a subharmonic below the avalanche frequency [12], special stability problems can be encountered in that case. This subject has been treated by Hines [13], and is not considered further here.

Second, since the approximate magnitude of the gain will be inversely proportional to the distance between the circuit (negative) and device operating points, the small-signal gain should peak at approximately 10 GHz where the curves nearly intersect. Then, since the distance between device and circuit points undergoes a smaller percentage variation with frequency when the RF voltage is large, increasing bandwidth accompanying reduced peak gain at larger levels of incident power is expected.

Finally, because the device susceptance increases with RF voltage, the frequency f_p at which the peak gain occurs will shift downward, while the amount of gain at the peak decreases as a result of an increase in input power level. Since the variation of device susceptance with RF voltage becomes larger near the avalanche frequency, this gain expansion below f_p becomes more pronounced as f_p approaches the avalanche frequency. Figs. 3–6 present the results of the point-by-point analysis of the amplifier whose *D–C* diagram was given in Fig. 2, i.e., amplifier example 1. For convenience, the device and circuit parameters are summarized in Table I. This device admittance was obtained from Greiling and Haddad's large-signal model [10].

Gain is given as a function of frequency for five levels of input power in Fig. 3. These are −30 dBm, which is a small-signal condition, 1, 10, 50, and 100 mW. As predicted from the *D–C* diagram, f_p occurs at approximately 10 GHz in the small-signal case, shifting to lower frequencies as the input power level is increased. At the same time, the response broad-

TABLE I

Device and Circuit Parameters for Amplifier Example I	
Diode	Si Read p^+nin^+
Avalanche Region Length	1 μm
Drift Length	4 μm
Bias Current Density (J_0)	500 A/cm^2
Junction Area	1×10^{-4} cm^2
Tuning Slug	32 Ω, λ/4 at 10 GHz
Slug Location	4 mm from diode flange

ens and saturates so that at an input power level of 100 mW, for example, 7 ± 0.5 dB of gain is predicted between 9 and 10.6 GHz. This would correspond to an output power level of approximately 0.5 W with the diode adding 400 mW to the input signal. Because the large-signal model for the device admittance does not permit the velocity of the drifting carriers to fall below the scattering limited value, the large-signal negative conductance, and hence the amplifier gain predicted here for large values of input power, is somewhat optimistic.

Fig. 4 presents information about the saturation and dynamic-range properties of the amplifier at several different frequencies, including f_p, $f_p \pm 200$ MHz, and $f_p \pm 400$ MHz. The gain expansion at frequencies below f_p is clearly evident here. It is also of particular interest to note that the input power level at which departure occurs from small-signal operation, and hence gain compression or expansion, is very much dependent on the frequency. This is a consequence of both the nature of the D–C interaction (in which respect it is similar to other narrow-band amplifiers), as well as the band-limited nature of the IMPATT negative conductance.

Fig. 5 is a plot of phase shift versus frequency for the same five levels of input power, while Fig. 6 presents phase-shift information as a function of input power at constant frequencies of 9.6, 9.8, 10, 10.2, and 10.4 GHz. It is of interest to note that both figures indicate the possibility of obtaining a phase shift relatively independent of input power at a constant frequency slightly above f_p.

III. Loading Circuit Characteristics

The ability to relate the D–C diagram to expected amplifier properties, as discussed previously, permits an ideal circuit to be defined in terms of the admittance behavior required in a load to obtain optimum broad-band stable reflection gain from a particular negative-conductance device. This usually requires that the real parts be related to one another by a multiplicative constant, with imaginary parts equal and of opposite sign throughout the frequency range over which the device conductance is negative. Stability requires that the reflection coefficient remains finite under all conditions of applied drive level; hence, for an IMPATT device, the real part of the circuit admittance must be larger than the magnitude of the real part of the device small-signal admittance. Fig. 7 presents a D–C diagram for the same device as in Fig. 2 with the admittance locus of such an ideal circuit shown. It is useful in that it presents a synthesis goal for the circuit designer, although its exact realization may be difficult, if not impossible, since the frequency dependence of the ideal circuit violates the classical requirement for lossless circuits whose

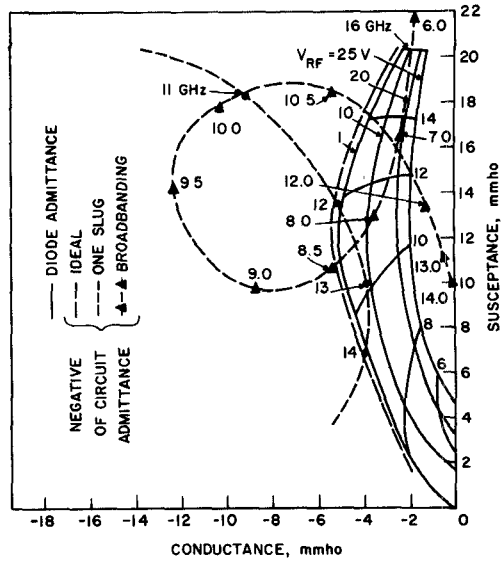

Fig. 7. D–C diagram for comparison of ideal and actual circuit admittances.

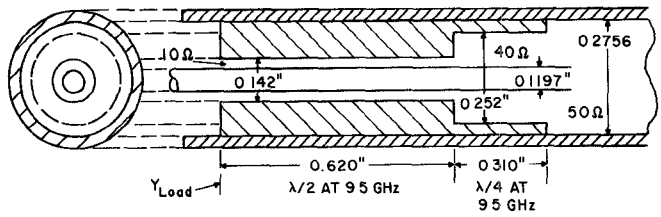

Fig. 8. Composite tuning slug for low-Q admittance pole.

driving-point susceptance must be an increasing function of frequency. Since the required circuit admittance does have a nonzero real part, the possibility of synthesizing a susceptance behavior which decreases with frequency exists over a limited frequency range near an admittance pole, although somewhat complicated tuning schemes are indicated for the simultaneous realization of the desired real- and imaginary-part behavior. With Q values such as are dictated by the choice of a center frequency near the peak small-signal negative conductance and stable high gain, the use of quarter-wave transformers in 50-Ω coaxial circuits generally leads to circuit behavior such as that shown by the curve labeled "negative of one slug circuit admittance." Although device and circuit curves intersect, they do not do so at a common frequency; hence, this is a stable case with high small-signal gain predicted near 12 GHz. Note that the susceptance behavior displays the opposite frequency dependence from the ideal circuit.

Finally, the curve labeled "negative of broad-banding circuit admittance" is the response calculated for a coaxial cavity with a composite slug such as shown in Fig. 8. The shape of this curve between 9 and 10 GHz approaches the desired behavior, and with impedance scaling would offer promise of relatively flat gain over that range. However, the shape of the locus above and below that frequency range would make a common frequency intersection probable at several points, e.g., near 8 and 10.5 GHz, and such a circuit would most likely be unstable. Most synthesis procedures for broad-band matching [14], [15] utilize multiple resonances in such

a fashion that several similar but smaller area loops occur adjacent to one another in the admittance plane.

IV. Power Addition and Gain in a Stable Reflection Amplifier

Under ideal conditions, the power which can be added to an input signal in a negative-resistance amplifier is equal to the maximum power which can be generated by the same device in a free-running oscillator [6], although the loading circuit admittance will differ for the two cases. The value of power gain when this maximum power addition takes place, however, is dependent upon the specific device $I-V$ relationship, and may differ for various kinds of negative-resistance devices, as well as for a specific device such as an IMPATT diode under different operating conditions. It will also depend upon the choice of the device material, doping profile, and circuit admittances at harmonic frequencies [11]–[13].

The theoretical determination of the maximum power which can be added by a negative-resistance device in a stable reflection amplifier and the gain level at which it takes place has been attempted by several authors [5], [7]. Their approach has generally involved assuming a specific instantaneous $I-V$ relationship for the device, after which the problem is straightforward. The approach here is to carry through the problem for a generalized functional relationship which can then be utilized to compare the results obtained from several different functional dependencies of diode immittance upon RF voltage and frequency.

Assume that $Y_{\text{device}}=G_{ss}+f(V)+j[B_{ss}+f_1(V)]$, where V is the peak value of sinusoidal RF voltage, and assume that $Y_{\text{load}}=kG_{ss}-jB_{ss}$ at the frequency for which the small-signal gain is a maximum. Here, G_{ss} and B_{ss} are the small-signal values of device conductance and susceptance, while $f(V)$ and $f_1(V)$ express their nonlinear dependence on RF voltage. Stability requires that $|k|>1$, gain requires that $G_{ss}<0$, and realizability of Y_{load} from passive components then requires that $k<0$. Then (1) may be expressed as

$$|\Gamma|^2=\left|\frac{G_{ss}(k-1)-f(V)+jf_1(V)}{G_{ss}(k+1)+f(V)+jf_1(V)}\right|^2. \tag{4}$$

Also, since the power generated by the device is given by $1/2$ Re $Y_{\text{device}}V_{\text{RF}}{}^2$, it may be written as

$$P_{\text{gen}}=\tfrac{1}{2}(G_{ss}V^2+f(V)V^2) \tag{5}$$

and this will be a maximum when $dP_{\text{gen}}/dV=0$. Taking the indicated derivative and setting it equal to zero results in

$$f(V_m)=-\left(G_{ss}+\frac{V_m}{2}f'(V)\,|_{V=V_m}\right) \tag{6}$$

and (6) is substituted into (4) resulting in

$$|\Gamma_M|^2=\left|\frac{kG_{ss}+\frac{V_m}{2}f'(V)\,|_{V=V_m}+jf_1(V_m)}{kG_{ss}-\frac{V_m}{2}f'(V)\,|_{V=V_m}+jf_1(V_m)}\right|^2 \tag{7}$$

where V_m is the RF voltage across the device which results in maximum generated power. $f'(V)|_{V=V_m}$ means df/dV evaluated at $V=V_m$ and may not be equal to zero for V_m to exist and remain finite. Since the peak small-signal gain is given by $\Gamma=(k-1)/(k+1)$, which results from (4) when $f(V)=f_1(V)=0$, it is seen that a large gain requires $k\approx -1$ so that in the limit, as the small-signal gain becomes very large, (7) may be taken as

$$|\Gamma_M|^2=\left|\frac{G_{ss}{}^2-G_{ss}V_m[f'(V)]_{V=V_m}+\frac{1}{4}V_m{}^2[f'(V)]_{V=V_m}+[f_1(V_m)]^2}{G_{ss}{}^2+G_{ss}V_m[f'(V)]_{V=V_m}+\frac{1}{4}V_m{}^2[f'(V)]_{V=V_m}+[f_1(V_m)]^2}\right|. \tag{8}$$

The above formulas have been programmed for solution on a digital computer under the assumption that $f(V)$ and $f_1(V)$ can be expressed as polynomials in V. These polynomials are constructed by solving a set of simultaneous equations formed from numerical data points determined by a large-signal analysis [11]. For the results presented here, five data points were used resulting in fourth-order polynomials. The smoothness of the polynomial approximation to the input points was examined by plotting values of G (conductance) and B (susceptance) obtained by solving $f(V)$ and $f_1(V)$ at closely spaced values of V_{RF}, and a well-behaved curve resulted over a range from 0.1 to 50 V. Plots of power added and gain as functions of RF voltage for values of small-signal gain equal to 10, 20, and 30 dB are produced for a given frequency. Figs. 9 and 10 show the results of such an analysis for a GaAs p^+-nn^+ X-band device biased at 500 A/cm^2 at 8 and 12 GHz, respectively.

Because of the marked dependence of susceptance on RF voltage near the avalanche frequency, the gain at 8 GHz saturates rapidly with increasing RF voltage and the gain at which maximum power is added to the input signal is found to be approximately 0.2 dB regardless of the small-signal gain. For an amplifier with 30 dB of small-signal gain, the gain is found to compress to 3 dB when the power added is approximately 20 mW.

In Fig. 10, which shows the power added and the gain behavior near the negative conductance peak at 12 GHz, it is shown that the maximum power added is approximately 700 mW and it occurs with 3 dB of gain in an amplifier tuned to provide 20 dB or more of small-signal gain.

Next, in Fig. 11, the predicted gain and power-addition relationship is shown for an Si p^+-nn^+ X-band diode at 12 GHz, where the peak negative conductance is obtained for a bias current density of 500 A/cm^2. It is of interest to note that Fig. 11 predicts a maximum of 500 mW of power addition at 3 dB of gain for an amplifier with a small-signal gain as low as 10 dB for this diode. This would result in 1 W of output power from such an amplifier.

In Fig. 12, the results are presented for the complementary Si structure—an n^+-pp^+ device. All other conditions remain the same. Because of the larger negative conductance generated by this complementary diode at low to moderate RF voltages, superior power-addition properties are predicted. At 12 GHz, 800 mW of generated power could be added in a stable amplifier at 3 dB of gain, yielding 1.6 W of output power when the amplifier is tuned for 10 dB of small-signal gain. For 30 dB of small-signal gain, nearly 800 mW is added at 6 dB of gain for an output power of approximately 1 W.

In summary, then, it appears that the p-type Si diode offers better saturation properties in a stable reflection ampli-

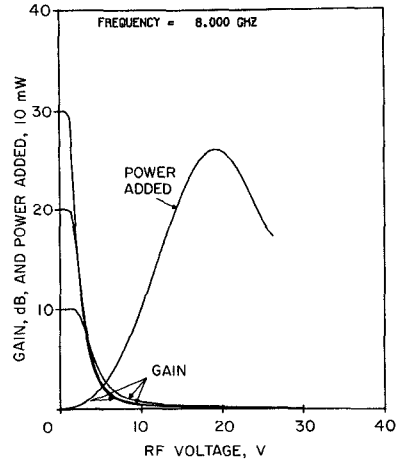

Fig. 9. Gain and power added by a GaAs p^+-nn^+ diode at 8 GHz.

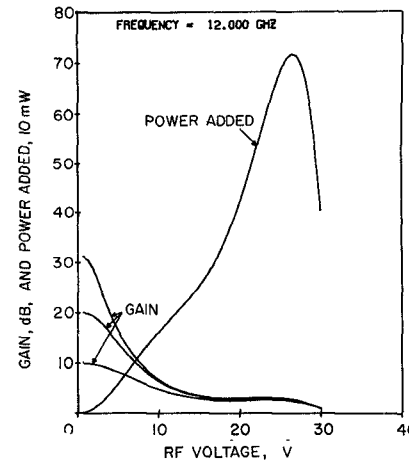

Fig. 10. Gain and power added by a GaAs p^+-nn^+ diode at 12 GHz.

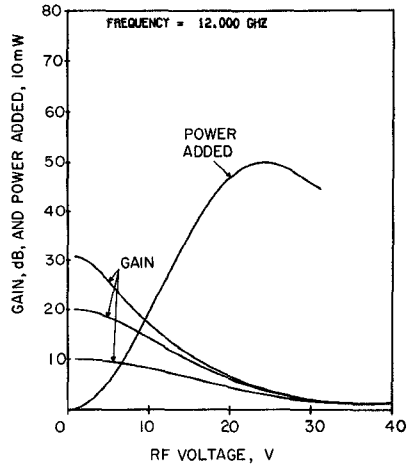

Fig. 11. Gain and power added in an Si p^+-nn^+ amplifier at 12 GHz.

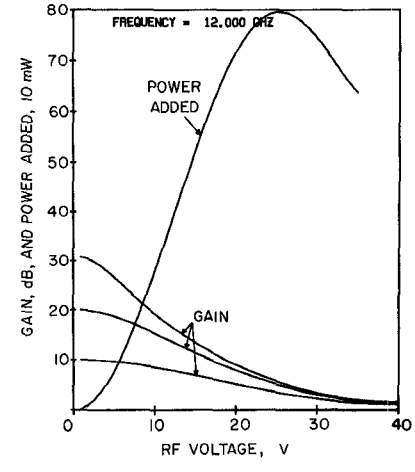

Fig. 12. Power added and gain from an Si n^+-pp^+ diode at 12 GHz.

fier circuit than either the n-type Si or GaAs device for center frequencies sufficiently above the avalanche frequency. For the n-type diodes, GaAs appears to be superior to Si, again for frequencies near the small-signal negative conductance peak. The results of this comparison at the higher frequencies, i.e., near the negative conductance peak, are consistent with the narrower avalanche region widths found in the p-type Si and the GaAs diodes [11]. In general, the narrower avalanche region width results in a higher negative conductance since the spread of transit angles about the optimum is smaller for carriers generated near each edge of the avalanche zone. Finally, these conclusions are valid only for the case of a stable amplifier wherein stability dictates a load admittance with a real part larger than the small-signal device negative conductance and the dependence of device admittance on RF voltage determines the gain which accompanies maximum power addition. For either free-running or injection-locked oscillators, the maximum power which can be generated by the device alone is a more realistic basis for comparison, and the GaAs device appears to be a better choice.

V. Broad-Banding Capability of IMPATT Devices

Differences in the small-signal device quality factor Q_d, defined as B_d/G_d, may be seen from the admittance characteristics of the various devices studied previously, which suggests that there are differences in the instantaneous fractional bandwidth of amplifiers employing these different devices. In this section, therefore, the optimum fractional bandwidth obtainable from each device is determined according to methods based on Bode–Fano matching techniques [14]–[17]. These are strictly applicable only when the device can be modeled by a frequency-independent shunt $-G$ and C. For amplifiers with a large value of small-signal gain, i.e., 30 dB, optimum fractional bandwidths are of the order of 5 percent, however, and the departure from constant values of device conductance and linear frequency dependence of device susceptance is not too great over this range. The realization of the ultimate bandwidth at lower gain levels dictates the synthesis of a circuit by means of a more complex lossy model for the device, such as proposed by Ku and Scherer [4].

According to the simpler method [14], fractional bandwidth w is given by g_1/Q_A, where g_1 is the susceptance of the first resonator in the matching network normalized by the value of negative conductance at the center frequency [15].

Q_A is given by $f_0/(f_a-f_b)$, where the f_i are frequencies defined as follows. The desired center frequency is f_0 and a shunt inductance is added to the device terminals to resonate the device there. The resonated device then has a susceptance $B_d'(f)$ which is negative below f_0 and positive above it. There is a frequency below f_0 and another frequency above it at which the $|B_d'(f)|$ and $|G_d(f)|$ are equal, and these two frequencies are f_a and f_b. Matthaei *et al.* [15] have shown that

TABLE II

BROAD-BAND CAPABILITIES OF SEVERAL SILICON STRUCTURES

Packaging	Gain (dB)	Ripple (dB)	Bandwidth w(%)	Frequencies (GHz) High	Middle	Low
Case I. Ideal Read Structure, p^+nip						
a. Not packaged	30	0.1	3.37	13.524	13.300*	13.076
b. " "	10	3.0	44.2	16.240	13.300	10.360
c. Package 023, coaxial	30	0.1	2.65	13.476	13.300	13.124
d. " " "	10	3.0	34.8	15.620	13.300	10.980
e. " " "	30	0.1	2.79	11.407	11.250**	11.093
f. " " "	10	3.0	36.6	13.310	11.250	9.190
Case II. Double-Drift Region Structure, p^+pnn^+						
a. Not packaged	30	0.1	3.7	12.629	12.400*	12.171
b. " "	10	3.0	48.7	15.410	12.400	9.390
c. Package 023, coaxial	30	0.1	2.5	12.555	12.400*,**	12.245
d. " " "	10	3.0	32.8	14.430	12.400	10.370
Case III. p-Type One-Sided Abrupt Junction, n^+pp^+						
a. Not packaged	30	0.1	3.18	13.715	13.500*	13.285
b. " "	10	3.0	41.8	16.300	13.500	10.700
c. Package 023, coaxial	30	0.1	2.61	13.676	13.500	13.324
d. " " "	10	3.0	34.2	15.800	13.500	11.200
e. " " "	30	0.1	2.17	12.484	12.350**	12.216
f. " " "	10	3.0	28.5	14.110	12.350	10.590
Case IV. n-Type One-Sided Abrupt Junction, p^+nn^+						
a. Not packaged	30	0.1	3.14	13.661	13.450*	13.239
b. " "	10	3.0	40.2	16.150	13.450	10.750
c. Package 023, coaxial	30	0.1	2.34	13.607	13.450	13.293
d. " " "	10	3.0	30.8	15.520	13.450	11.380
e. " " "	30	0.1	2.43	12.020	11.875**	11.730
f. " " "	10	3.0	31.8	13.265	11.875	10.485

* $|-G_{device}| = \max.$
** $|jX_{term}| = 0.$

TABLE III

DIODE STRUCTURES STUDIED FOR BROAD-BAND CAPABILITY

Diode	Material	Profile	Bias Current Density (A/cm^2)	Active Region Length (μm)	Doping, Active Region
Ideal Read	Si	n^+pip^+	440	4	3.75×10^{16} to 1×10^{14}
p-type	Si	n^+pp^+	500	5	5×10^{15}
n-type	Si	p^+nn^+	500	5	5×10^{15}
Double-Drift Region (DDR)	Si	p^+pnn^+	500	8.875	5×10^{15}
n-GaAs	GaAs	p^+nn^+	500	2.9	1×10^{16}

when the susceptance added to resonate the diode at the desired center frequency, whose value is determined by the device susceptance alone, is considered to be the first element in the broad-banding network and is used to select a broad-banding network, the optimum bandwidth is obtained with the gain and ripple dictated by this choice. On the other hand, the design for a specified gain and ripple in general may require a value for the first element in the broad-banding network which is different from that producing the optimum w. As an absolute figure of merit, the optimum fractional bandwidth may lead to values of gain which are very low. Getsinger's Figs. 3–5 indicate that gain decreases and ripple increases with increasing values of g_1 [14]. Since $w = g_1/Q_A$, the gain and optimum fractional bandwidth tend to vary somewhat inversely with one another and a meaningful comparison of device broad-banding properties should be carried out for equal values of gain and ripple. This has been done using room-temperature admittance data for several selected frequencies in Si devices, and the results are given in Table II both for unpackaged and packaged devices. The frequencies selected for comparison were those where the negative conductance achieved its peak value and those where the package parasitics resonated the device giving the minimum achievable reactance. Table II indicates that the double-drift structure provides the maximum broad-banding capability followed by the ideal Read, p-type, and n-type structures in that order for unpackaged devices, and that the package impedance transformation in the coaxial circuit reduces the instantaneous bandwidth which can be obtained by 20–30 percent for each structure. Significant properties of the device structures studied are summarized in Table III.

Broad-banding capability has also been investigated for p-type Si and n-type Si and GaAs one-sided abrupt junctions at several different bias current densities and at elevated temperatures which correspond more closely to actual operating conditions for normally encountered values of thermal resistance and forced air or water cooling. In order to permit device comparison versus frequency, the factor $1/Q_A$ is used as a figure of merit in this section. Since w is given by g_1/Q_A and g_1 is fixed for a given gain, ripple, and degree of reactive multiplicity in the broad-banding network, curves of $1/Q_A$ as a function of frequency provide a direct comparison of instan-

taneous fractional bandwidth for a fixed gain and ripple. Fig. 13 shows the factor $1/Q_A$ versus frequency for the n-type Si diode at 500 and 1000 A/cm² at room temperature, 500 A/cm² at 100°C, and 1000 A/cm² at 200°C. The device structure is the same as that studied in the previous section except for the elevated temperatures in which the n-region width has been reduced to 3.5 μm in order to retain a negative conductance peak near 12 GHz. It is shown in Fig. 13 that the broad-banding capability is improved by increased values of bias current, although the improvement is not as great when the rise in temperature which accompanies higher current levels is considered. Similar behavior is observed for the p-type Si and the n-type GaAs diodes, as is shown in Fig. 14. It should be pointed out, however, that the GaAs structure for this case is identical at both temperatures; hence, the broad-banding capability as measured by $1/Q_A$ peaks at a lower frequency for the elevated temperature data. The low-frequency end of each curve on Fig. 14 is located just above the appropriate avalanche frequency.

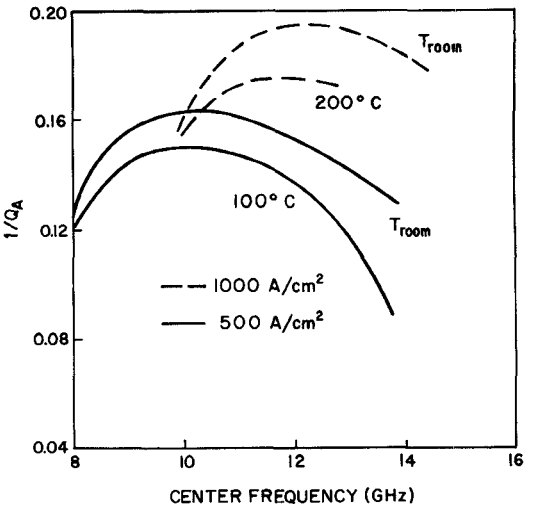

Fig. 13. Broad-band capability of an n-type Si diode as a function of frequency for several temperatures and bias current densities.

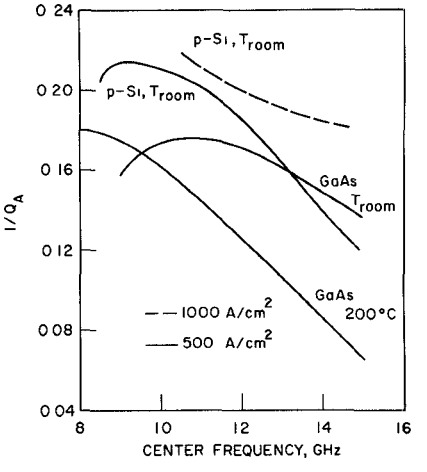

Fig. 14. Broad-band capability as a function of frequency for GaAs and p-type Si diodes at several temperatures and bias current densities.

In summary, it appears that the maximum useful gain bandwidth is obtained from the double-drift device at bias current densities as large as can safely be accommodated and that heating effects at the junction are deleterious with regard to instantaneous bandwidth. This means that low values of thermal resistance contribute to the broad-banding capability, as well as to the power-addition properties of avalanche-diode amplifiers.

Finally, the departure from a constant negative conductance and linear susceptive frequency behavior for realistic IMPATT admittance data means that calculated bandwidths in excess of 5–10 percent cannot be synthesized by the simple methods referenced here [14], [15] without significant response degradation near the band edges. An example of broad-banding results which can be obtained by these simple methods and a measure of the response degradation is given next, where the prototypes tabulated by Getsinger [14] are utilized to select a broad-band matching network for an n^+-pp^+ Si diode, and the gain of such an amplifier is calculated and plotted as a function of frequency for several values of input power such that both small- and large-signal saturated operation are analyzed.

For this example, the p-type Si X-band diode previously investigated for power adding and broad-banding capability is utilized. The p-region is 5 μm wide and is doped at 5×10^{15} cm^{-3}. Bias current density is 500 A/cm² and room-temperature operation is assumed. The considerations discussed previously indicate good power-adding and broad-banding capability at 11 GHz, as well as a reasonably constant negative conductance over a range of frequencies on either side for this device, and therefore a center frequency f_0 of 11 GHz is chosen. Unpackaged device data are utilized which imply that the package will be designed to constitute part of the broad-banding network, or that an unpackaged design such as MIC will be utilized. A shunt inductance of 0.976 nH is required to resonate the 14.8 mmho of small-signal device susceptance at 11 GHz. Obviously, an ideal lumped inductor in shunt with the device would present bias circuit difficulties, although it might be realized in a distributed circuit, for example, by means of a shunt open-circuited stub. The normalized susceptance of this first resonating element is the minimum value of g_1 which can be added in an optimum gain-bandwidth configuration. Next, the 14.8 mmho of susceptance is normalized by 7.3 mmho of negative conductance at the 11-GHz design frequency giving a g_1 (minimum) of 2.03. Getsinger's Fig. 4 indicates that a minimum gain of 10 dB with an added ripple of 1.5 dB may be obtained from a three-resonator design with a value of approximately two for g_1 [14]. The fractional bandwidth obtainable from such a design would be given by g_1/Q_A, and for Q_A determined to be 4.980 from the data of Fig. 14, a predicted value of 0.408 or approximately 40 percent results for w. A gain response curve of 10.75 ± 0.75 dB would then be predicted from 9 to 13 GHz. However, significant degradation of the gain is to be expected near the band edge. This can be seen clearly from a consideration of the frequency dependence of B_d at small-signal operation. For a fractional bandwidth of 0.40, linear frequency dependence would give a B_d of 17.6 mmho at 13.2 GHz and 12 mmho at 8.8 GHz. Inspection of device admittance data [10] yields 24 and 5 mmho, respectively, for the approximate actual values. A smaller value for w permits the choice of a network providing a higher midband gain, and as a compromise the case of $n=3$, $w=0.30$, minimum gain = 20 dB, and ripple = 0.5 dB is utilized to select normalized prototype values from Getsinger's Table 1. This gives $g_1=2.038$, $g_2=0.726$, $g_3=1.328$, and $g_4=0.580$, where g_1 and g_3 are normalized shunt susceptance prototypes, g_2 is a normalized series reactance, and g_4 is the normalized series load resistance. Conver-

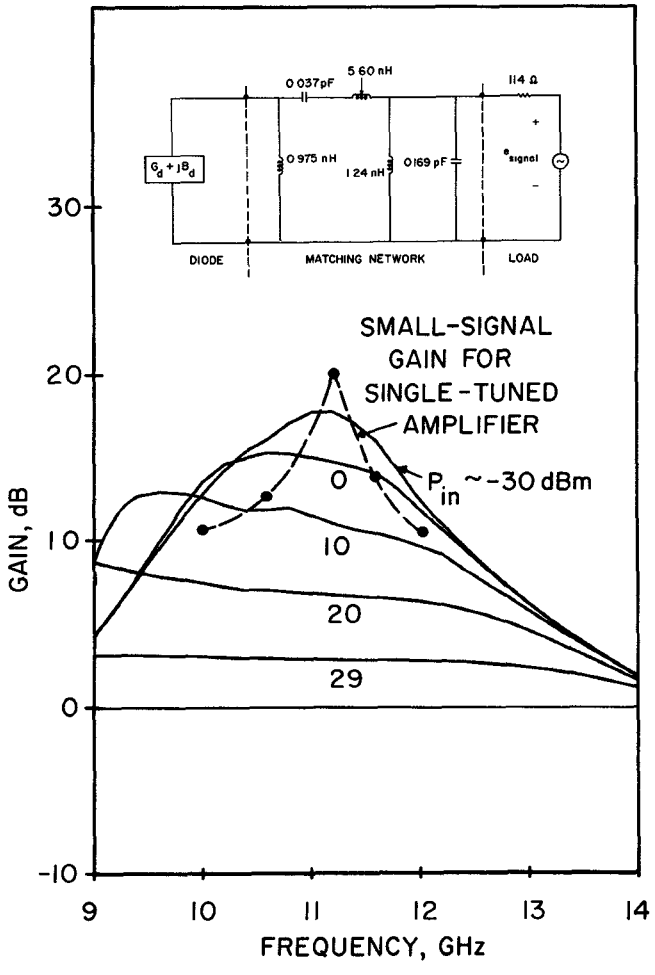

Fig. 15. Gain versus frequency for broad-banding examples at several input power levels.

TABLE IV

PARAMETERS MEASURED FOR AN Si (D5968F-6) AND A GaAs (562SIC-24) *X*-BAND IMPATT DIODE

Material	GaAs	n-Si
N_d	1×10^{16} cm^{-3}	5×10^{15} cm^{-3}
d	2.75 μm	3.5 μm
A	1.7×10^{-4} cm^2	1.0×10^{-4} cm^2
$C_{j_{V=V_B}}$	0.75 pF	0.36 pF
$V_{B_{\text{room temp}}}$ (I = 1 mA)	50 V	67 V
R_s	2.50 Ω	3 Ω
L_s	0.70 nH	0.64 nH
L_{s2}	0.30 nH	0.47 nH
C_p	0.14 pF	0.24 pF
C_{p_2}	0.13 pF	0.04 pF

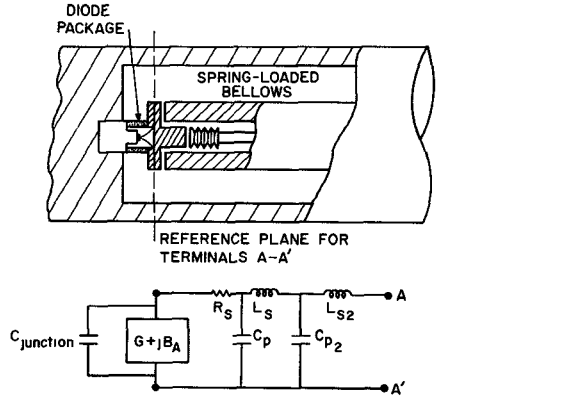

Fig. 16. Lumped-element configuration for package/mount transformation equivalent circuit.

sion of the prototype to a bandpass matching network is straightforward and leads to a network similar to that shown in the inset of Fig. 15. The final values of the elements shown were obtained by minor adjustments to the values obtained from Getsinger's prototype in order to level the resulting response curve. This is a somewhat empirical adjustment to compensate for the nonconstant value of G_d and C_d with frequency, and consisted of raising the resonant frequency of the parallel LC combination in the shunt branch at the right-hand side of the figure. Several techniques for the realization of the lumped-element prototypes by means of distributed circuits are given by Matthaei *et al.* [15].

Values of gain versus frequency for input power levels of −30, 0, 10, 20, and 29 dBm have been computed for the p-type diode in this lumped-element matching circuit, and this information is plotted in Fig. 15 along with a small-signal curve for the singly resonated device without the additional broad-banding resonators. Significant improvement is shown for the broad-band case, although the nonlinearity of device admittance results in a response which is somewhat degraded from the calculated ideal case as expected. The result is 16 dB ± 2 dB over approximately a 16.5-percent bandwidth centered near 11 GHz. The further broadening of response with increasing input power is also noteworthy. A gain of 3 dB ± 0.3 dB is predicted at an input power level of 800 mW from 9 to 12 GHz yielding an output power of more than 1.5 W. This is, of course, consistent with the power-added versus gain study discussed previously.

VI. Experimental Results

Determination of the avalanche-diode structure, doping profile, and package parasitic element properties can be carried out with a nondestructive procedure based upon measurements of diode capacitance as a function of reverse voltage [10], [18], [19] and impedance versus frequency [10], [20], [21] in a desired mounting configuration. The results of such procedures for the determination of device and equivalent-circuit parameters are shown in Table IV and Fig. 16 for the two diodes utilized to obtain the data presented in this section. In addition, the admittance of an avalanching diode displays a strong dependence upon temperature [11] and because several hundred kilowatts per square centimeter are dissipated at the junction under normal operating conditions, it becomes necessary to obtain admittance data corresponding to a chosen bias current density and the junction temperature it will produce under given heat-sinking conditions. Since the breakdown voltage varies approximately linearly with temperature, it provides a measure of junction

TABLE V

TEMPERATURE VARIATION OF SILICON PARAMETERS

Parameter	300°K		200°C		250°C	
	Electrons	Holes	Electrons	Holes	Electrons	Holes
v_{sat} (cm/s)	1.02×10^{7}	1.20×10^{7}	8.5×10^{6}	1.02×10^{7}	7.2×10^{6}	7.2×10^{6}
Ionization Rates						
$\alpha = A\, e^{-(b/E)}$						
A (cm^{-1})	3.8×10^{6}	2.25×10^{7}	1.8×10^{6}	1.0×10^{7}	1.08×10^{6}	0.71×10^{7}
b (V/cm)	1.75×10^{6}	3.26×10^{6}	1.64×10^{6}	3.2×10^{6}	1.61×10^{6}	3.18×10^{7}

temperature. A temperature coefficient of approximately 1 V/11.6°C was measured for the Si abrupt junction and a space-charge resistance of approximately 40 Ω was obtained from a pulsed I–V measurement using 2-μs pulses at a 5-kHz pulse-repetition rate. This information makes it possible to monitor the junction temperature while operating the amplifier. Admittance data for temperatures other than room temperature and 200°C are not readily available, however, since behavior of saturated drift velocities and ionization rates for holes and electrons is not well known as a function of temperature. All of the preceding considerations led to a choice of operating parameters wherein the device was intended to be operated at 200°C and 1000 A/cm². Because of the thermal resistance of the path to the heat sink, the actual conditions obtained corresponded to 250°C and 950 A/cm². Device admittance data were obtained from the large-signal model of Schroeder and Haddad [11] using the ionization rates and saturated drift velocities for the actual conditions as given in Table V. The values for 300 K and 200°C are those collected by Schroeder and Haddad [11], while the values at 250°C have been obtained by linearly extrapolating from the other two temperatures and then applying an empirically determined saturation factor of 10 percent.

The amplifier was tuned to provide approximately 14 dB of small-signal gain with 1 dB of ripple between 9.350 and 9.530 GHz using two coaxial tuning slugs. Both slugs were 0.300 in long with an outer diameter of 0.265 in and an inner diameter of 0.195 in. Both slugs had their outer circumference covered by a single 0.005-in thickness of Teflon tape. The closest face of the first slug was located 0.060 in from the diode flange, while the equivalent dimension for the second slug was 0.527 in. Under these conditions, curves of gain versus frequency were obtained at input power levels of −10, 0, 7, 10, 16, 20, and 23 dBm. No subharmonic oscillations occurred at input power levels below 20 dBm, although at this level 4.5 GHz was present when the input was swept through 9 GHz. At 23 dBm of input power, a subharmonic at 4.7 GHz was induced by a 9.4-GHz signal at the input, as well as the 4.5 and 9.0 pair described earlier. Gain was measured relative to a 0-dB reference obtained by replacing the cavity with a coaxial short.

After these measurements had been completed, the circuit impedance was measured without changing the position of the tuning slugs by means of a coaxial adapter which replaces the diode and cavity end wall. This permits the determination of the impedance seen by the packaged diode at its reference flange. This impedance was then transformed through the equivalent circuit described in Fig. 16 and Table IV.

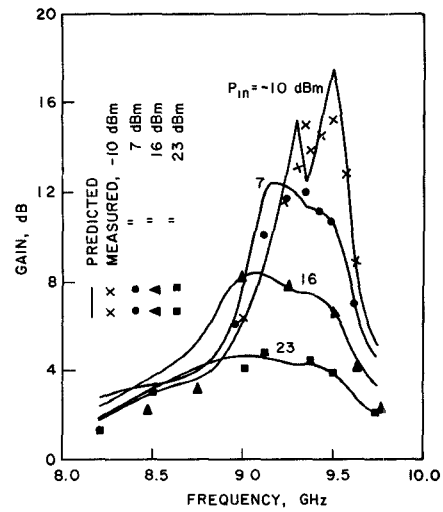

Fig. 17. Comparison of predicted and measured values of gain versus frequency for various input powers (Si diode D5968F-6).

Fig. 17 indicates both the theoretical and measured behavior of the amplifier after one small modification was made in the value of R_s—the series loss in the equivalent circuit. In order to obtain the correct value of the small-signal gain at the peak, R_s was increased to 6 Ω. This value seems rather high when only undepleted substrate and lead wire resistance in the device and its package are considered. However, the additional 3 Ω is a reasonable value associated with the low-Q resonant cavity losses formed by the diode and tuning slugs in the coaxial circuit. Removal of the diode and cavity end wall to measure the impedance presented by the circuit could, of course, change the field patterns in the end of the cavity, and therefore this additional loss might not appear in the circuit impedance measurement. Such an adjustment in R_s resulted in the excellent agreement between calculated and measured response and saturation properties shown in Fig. 17. The ripple effect at the small-signal level near 9.3 GHz is a result of a kink in the measured circuit admittance near that frequency and is believed to be attributable to the small but finite VSWR contributed by the circulator several wavelengths away from the diode.

Next, a series of measurements was carried out on a p^+-nn^+ GaAs device identified as diode 562SIC-24 for the purpose of verifying the theoretical work described previously for this material as well as Si. For this case, the space-charge resistance and temperature coefficient of breakdown voltage were determined to be 30 Ω and 12°C/V, respectively, and a bias current density of 1000 A/cm² resulted in a junction temperature of 260°C. RF admittance data were obtained

using an ionization rate expression:

$$\alpha = 2.33 \times 10^5 \exp\left[-\left(\frac{7.07}{E}\right)^2\right]$$

for both holes and electrons. Here, α is the ionization rate or number of electron-hole pairs generated by one carrier per centimeter traveled and E is the electric field strength in kilovolts per centimeter. The constants 2.33×10^5 and 7.07 were obtained by linear extrapolation to 260°C from data collected by Schroeder and Haddad [11] for operation at 300 K and 200°C as was the value of saturated drift velocity—5.45×10^6 cm/s.

A small-signal gain of 20 dB at 8.725 GHz was obtained using two Teflon coaxial tuning slugs as shown in the inset of Fig. 18. This figure shows the calculated gain for such an amplifier with measured data shown as points near the respective curves for several levels of input power. The agreement was good until the input power level of 13 dBm was reached, at which time the measured response had saturated beyond the level which was predicted. This could have been an effect of subharmonic loading, for the amplifier was on the verge of induced subharmonic oscillation at this level and higher levels of input power produced strong oscillations at approximately 4.3 GHz. No subharmonic lines were visible on the spectrum analyzer when the input power was 13 dBm or less, although a noisy signal at this frequency near the sensitivity threshold of the analyzer would have been difficult to detect.

Finally, the rate of saturation is strongly influenced by the value of R_s—the series resistance in the equivalent circuit of Table IV. The value of 3 Ω which was utilized in this case produced a good match under small-signal conditions when a diffusion coefficient of 50 cm²/s was used to obtain admittance data. There is a good deal of uncertainty surrounding the correct value of diffusion coefficient [11] for GaAs, and, in addition, because of computation time, the admittance data were obtained assuming a field-independent value for this parameter. The choice of a smaller value of diffusion coefficient would have increased the small-signal negative conductance which would dictate a slightly larger value of R_s in order to predict the 20 dB of peak small-signal gain. This larger value of R_s would then have increased the degree of saturation at the higher power levels. For example, no diffusion would require a choice of $R_s = 8$ Ω to provide the correct small-signal gain, and, with $R_s = 8$ Ω and all other parameters the same, the calculated gain at an input level of 23 dBm would be approximately 5 dB which is 1 dB less than the measured value at the peak.

It is also noteworthy that the circuit admittance for this case was obtained by calculation using measured dimensions of the cavity and slugs instead of by direct impedance measurement, as was the case for the Si device experiment described in the previous section. For the calculation, the discontinuity capacitances associated with the air–dielectric interface at the faces of each slug were assumed to be negligible.

VII. Response Dependence on Bias Current Density

In this section, the dependence of gain and saturation properties are measured for a Si diode at several bias current densities under nonisothermal conditions when the circuit tuning is changed to provide approximately equal values of small-signal gain and frequency.

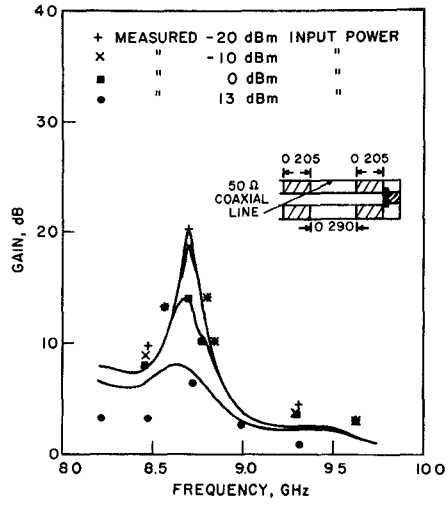

Fig. 18. Calculated and measured gain response of a GaAs amplifier (diode 562SIC-24).

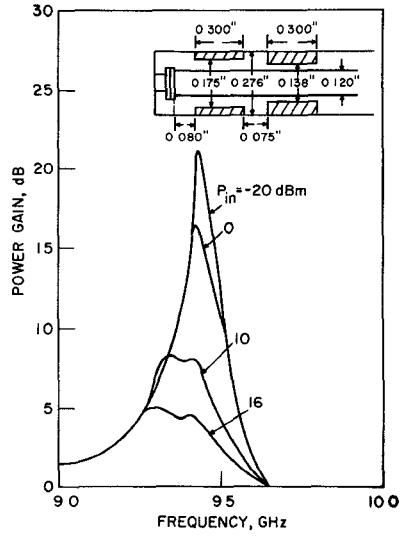

Fig. 19. Gain versus frequency at 500 A/cm² for an Si p⁺-nn⁺ diode.

In the first case, 21 dB of small-signal gain at 9.4 GHz was obtained with a bias current density of 500 A/cm². Tuning was accomplished with two coaxial slugs and the appropriate dimensions are shown, along with the plots of gain versus frequency, in Fig. 19 for input power levels of −20, 0, 10, and 16 dBm. The bias current density was then increased to 1000 A/cm² and a new tuning condition was obtained which produced 19 dB of small-signal gain at 9.2 GHz. Circuit dimensions and gain versus frequency for the same input power levels— −20, 0, 10, and 16 dBm—are shown in Fig. 20.

Several differences in amplifier properties are evident from the data shown in Figs. 19 and 20. At the lower current density, the gain compression between the small-signal drive and the input power level of 40 mW was 16 dB, while the shift in f_p was approximately 125 MHz toward the lower frequency end. At the higher current density the gain compressed by 11.5 dB between small-signal and 40-mW input power levels. Thus the output power at this drive level was approximately 5 dB higher for the 1000-A/cm² bias condition, and the RF conversion efficiency was approximately 2.7 percent versus 1.5 percent for the 500-A/cm² case.

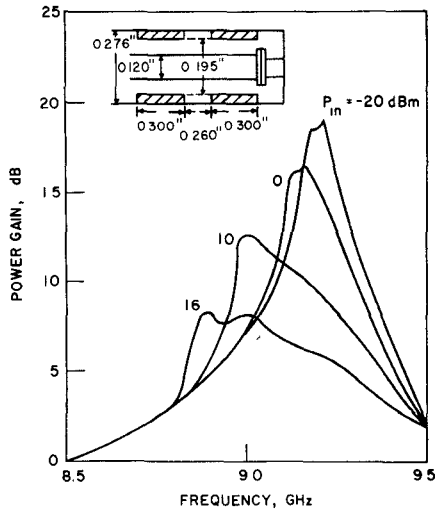

Fig. 20. Gain versus frequency at 1000 A/cm² for an Si p^+-nn^+ diode.

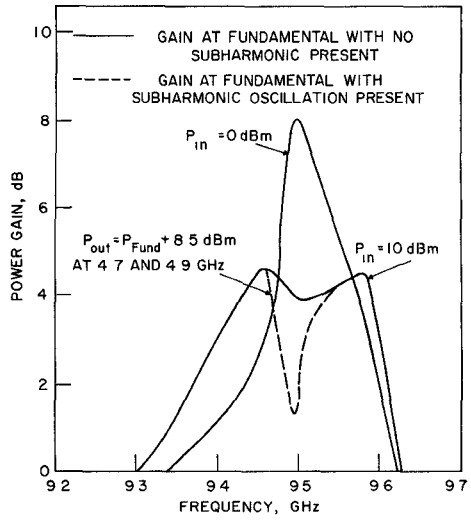

Fig. 21. Power gain versus frequency with subharmonic tuning.

Next, because the avalanche frequency increased approximately as the square root of the bias current density, f_p was closer to the avalanche frequency at the higher current density. Thus the shift downward in frequency with increasing drive levels was more pronounced and was approximately 300 MHz for an input signal of 16 dBm.

Finally, the instantaneous bandwidth, and therefore the gain-bandwidth product, was significantly larger for the higher current density case at all levels of input power. This is, of course, consistent with the theoretical predictions discussed previously.

VIII. Operation at High Output Power Levels

The most frequently occurring limitation on output power during the experimental work described here was the reduction in gain which accompanied the onset of subharmonic oscillation at the higher levels of input power. This widely observed phenomenon, shown in Fig. 21, is consistent with theoretical observations concerning multifrequency operation [22] of IMPATT devices and indicates the importance of presenting the proper load admittance at frequencies near the subharmonic of the intended operating range.

Most circulators are rather narrow-band devices with high VSWR's out of band. Thus a reactive termination at the subharmonic is difficult to avoid in a circulator-coupled reflection amplifier. The use of quarter-wave transformers, or coaxial tuning slugs, to tune out the out-of-band reactance of a circulator has been attempted. Since these are one-half wavelength at the fundamental, they are transparent to that frequency in the ideal case and should not affect the tuning in the desired band. Such a scheme can be successfully employed over narrow frequency ranges; however, it has proven difficult to suppress subharmonic oscillation without affecting tuning at the fundamental throughout the band of frequencies over which relatively flat large-signal gain is otherwise obtainable.

Broad-band circulation encompassing both the subharmonic and fundamental frequencies in the passband has been obtained with a miniature three-port coaxial circulator. This commercially available component was found to have a VSWR less than 1.5 at all ports with a consistent direction of circulation and isolation between 4 and 10 GHz. Thus a fundamental in the lower half of X-band had its subharmonic

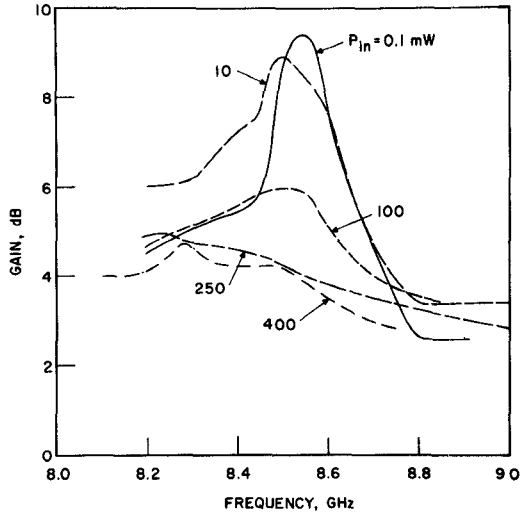

Fig. 22. Power gain versus frequency for a GaAs diode amplifier for different input power levels.

terminated nonreactively. It is also very important to ensure that low VSWR's at the subharmonic are presented at the output, input, or both ports of this circulator. For example, the use of waveguide components at these two ports will reflect the subharmonic causing it to be recirculated back to the diode. Such a feedback loop would favor the buildup of oscillations at the subharmonic. The use of a four-port circulator with a tunable termination in the circulation path from output back to amplifier input would eliminate this source of subharmonic instability. For the experimental work described here, a 6-dB coaxial attenuator was placed at the output of the three-port circulator and considered to be part of the load. This presented a VSWR of approximately 1.25 at the subharmonic and reduced the tendency for subharmonic oscillation sufficiently so that it was not present at drive levels as high as 26 dBm in several cases. When waveguide components were connected immediately adjacent to both ports, subharmonic oscillation was induced at input power levels of the order of 13 dBm. Fig. 22 is representative of experimental results in which output power levels of 1 W CW were obtained. For this case, the diode was an X-band GaAs Schottky-

barrier device biased at approximately 700 A/cm² loaded by two 30-Ω 8-GHz λ/4 coaxial slugs spaced approximately one-quarter wavelength at f_p with the first slug very near the diode flange. This tuning condition produced a small-signal gain of approximately 10 dB at 8.5 GHz. The input power could be increased to 400 mW which was limited by the ability of the driving source to provide a reasonably level (±1 dB) swept frequency output. At this level of input power, the gain decreased to approximately 4.5 dB at 8.3 GHz and 4 dB or better, which corresponded to 1 W of CW output power, was obtained between 8.1 and 8.55 GHz. The peak RF conversion efficiency was 7.1 percent.

IX. Summary and Conclusions

The purpose of this paper has been the presentation of an improved understanding of the design and analysis of microwave reflection amplifiers employing the negative-resistance property of IMPATT devices in order that the properties of such amplifiers might be examined in detail both theoretically and experimentally.

An examination of the complex expression for the reflection coefficient at a pair of terminals has led to the development of a semigraphical analysis which employs a *D–C* diagram to provide a qualitative measure of insight into reflection amplifier stability, gain, bandwidth, and saturation properties. This concept has also been utilized to define the admittance behavior of an ideal loading circuit for a reflection amplifier. Programs have been developed which utilize the digital computer to calculate gain, phase shift, and output power as functions of frequency and input power, as well as the variation of gain and power added with RF voltage. These programs require knowledge of device and circuit admittances at several discrete RF voltages and frequencies. Classical methods for comparing broad-banding capability on the basis of device small-signal admittance have been shown to be useful for IMPATT devices.

The theoretical concepts developed for the investigation have been utilized to study the dependence of amplifier response on doping profile, bias current density, temperature, and circuit design. It has been shown that the Si n^+-pp^+ device is theoretically capable of providing output powers in excess of 1.5 W at a gain of 3 dB in a stable amplifier circuit near the optimum frequency. Gain bandwidth and power added are both shown to be enhanced by higher current densities, although both are degraded somewhat by the higher junction temperatures which normally accompany the higher current levels. The double-drift region Si diode offers the largest gain-bandwidth product of the structures investigated, and is likely to provide excellent power-adding properties as well, although the unavailability of large-signal admittance data for this structure prevents the detailed study of that property. Multiple tuning has been shown to be an effective method of broadbanding this class of amplifiers, although nonlinearities in device admittance cause a departure from theoretical values of the gain-bandwidth product for fractional bandwidths larger than approximately 5 percent.

Experimental measurements of gain as a function of frequency and input power level have been carried out utilizing Si and GaAs diodes, and excellent agreement has been demonstrated between theory and measurement. Additional experimental results have been presented which demonstrate the dependence of gain and bandwidth on bias current density and circuit tuning conditions.

References

[1] L. S. Napoli and R. J. Ikola, "An avalanching silicon diode microwave amplifier," *Proc. IEEE* (Corresp.), vol. 53, pp. 1231–1232, Sept. 1965.

[2] D. M. Snider, "A one-watt CW high-efficiency *X*-band avalanche-diode amplifier," *IEEE Trans. Microwave Theory Tech.* (Corresp.), vol. MTT-18, pp. 963–967, Nov. 1970.

[3] T. P. Lee, R. D. Standley, and T. Misawa, "A 50-GHz silicon IMPATT-diode oscillator and amplifier," in *1968 IEEE Int. Solid-State Circuits Conf. Digest* (Philadelphia, Pa., Feb. 1968), pp. 156–157.

[4] W. H. Ku and E. F. Scherer, "Gain-bandwidth optimization of avalanche-diode amplifiers," *IEEE Trans. Microwave Theory Tech. (Special Issue on Microwave Circuit Aspects of Avalanche-Diode and Transferred Electron Devices)*, vol. MTT-18, pp. 932–942, Nov. 1970.

[5] M. E. Hines, "Negative-resistance diode power amplification," *IEEE Trans. Electron Devices*, vol. ED-17, pp. 1–8, Jan. 1970.

[6] E. F. Scherer, "Large-signal operation of avalanche-diode amplifiers," *IEEE Trans. Microwave Theory Tech. (Special Issue on Microwave Circuit Aspects of Avalanche-Diode and Transferred Electron Devices)*, vol. MTT-18, pp. 922–932, Nov. 1970.

[7] C. W. Lee, "High power negative resistance amplifiers," *Microwave J.*, vol. 15, pp. 29–37, Feb. 1972.

[8] W. C. Tsai and C. W. Lee, "A *C*-band all ferrite integrated wideband high power GaAs avalanche diode amplifier," in *1972 IEEE-GMTT Int. Microwave Symp. Digest* (Arlington Heights, Ill., May 1972), pp. 179–181.

[9] W. T. Read, "A proposed high frequency negative resistance diode," *Bell Syst. Tech. J.*, vol. 37, pp. 401–446, Mar. 1958.

[10] P. T. Greiling and G. I. Haddad, "Large-signal equivalent circuits of avalanche transit-time devices," *IEEE Trans. Microwave Theory Tech. (Special Issue on Microwave Circuit Aspects of Avalanche-Diode and Transferred Electron Devices)*, vol. MTT-18, pp. 842–853, Nov. 1970.

[11] W. E. Schroeder and G. I. Haddad, "Nonlinear properties of IMPATT devices," *Proc. IEEE*, vol. 61, pp. 153–182, Feb. 1973.

[12] ——, "Effect of harmonic and subharmonic signals on avalanche-diode oscillator performance," *IEEE Trans. Microwave Theory Tech.* (Corresp.), vol. MTT-18, pp. 327–331, June 1970.

[13] M. E. Hines, "Large-signal noise, frequency conversion, and parametric instabilities in IMPATT diode networks," *Proc. IEEE*, vol. 60, pp. 1534–1548, Dec. 1972.

[14] W. J. Getsinger, "Prototypes for use in broadbanding reflection amplifiers," *IEEE Trans. Microwave Theory Tech.*, vol. MTT-11, pp. 486–497, Nov. 1963.

[15] G. L. Matthaei, L. Young, and E. M. T. Jones, *Microwave Filters, Impedance Matching Networks, and Coupling Structures*. New York: McGraw-Hill, 1964.

[16] H. W. Bode, *Network Analysis and Feedback Amplifier Design*. New York: Van Nostrand, 1945.

[17] R. M. Fano, "Theoretical limitations on the broadband matching of arbitrary impedances—Part I," *J. Franklin Inst.*, vol. 249, pp. 57–83, Jan. 1950.
——, "Theoretical limitations on the broadband matching of arbitrary impedances—Part II," *J. Franklin Inst.*, vol. 249, pp. 139–155, Feb. 1950.

[18] C. O. Thomas, D. Kahng, and R. C. Manz, "Impurity distribution in epitaxial silicon films," *J. Electrochem. Soc.*, vol. 109, pp. 1055–1061, Nov. 1962.

[19] I. Amron, "Errors in dopant concentration profiles determined by differential capacitance measurements," *Electrochem. Technol.*, vol. 5, pp. 94–97, Mar.–Apr. 1967.

[20] W. J. Getsinger, "The packaged and mounted diode as a microwave circuit," *IEEE Trans. Microwave Theory Tech.*, vol. MTT-14, pp. 58–69, Feb. 1966.

[21] I. W. Pence, "Impedance of packaged Gunn diodes and parametric circuit applications," Ph.D. dissertation, Univ. Michigan, Ann Arbor, 1970.

[22] M. E. Hines, "Special problems in IMPATT diode power amplifiers," in *1972 IEEE Int. Solid-State Circuits Conf. Digest* (Philadelphia, Pa., Feb. 1972), pp. 34–35.